J Solid State Electrochem (2016) 20:2363–2372
DOI 10.1007/s10008-016-3254-z

ORIGINAL PAPER

Influence of Ni^{2+} and Sn^{4+} substitution on gas sensing behaviour of zinc ferrite thick films

S. P. Dalawai[1] · T. J. Shinde[2] · A. B. Gadkari[3] · P. N. Vasambekar[1]

Received: 26 February 2016 / Revised: 13 May 2016 / Accepted: 17 May 2016 / Published online: 26 May 2016

Abstract Nanocrystalline ferrite powders of $Ni_xZn_{1-x+y}Fe_{2-2y}Sn_yO_4$ (x = 0, 0.2, 0.4, 0.6, 0.8, 1.0 and y = 0.1, 0.2) were prepared by oxalate co-precipitation method and characterized by XRD, FT-IR and FE-SEM techniques. The ferrite thick films (FTFs) of all compositions were prepared by screen printing technique and tested for gas sensing behaviour for liquid petroleum gas (LPG), ethanol (C_2H_5OH) and chlorine (Cl_2). For LPG, the sensitivity decreases with an increase in Ni^{2+} up to $x = 0.6$. It increases slightly for further increment in Ni^{2+}. For this gas, the sensitivity is higher for higher concentration of Sn^{4+} ($y = 0.2$) while the optimum temperatures are smaller than that for lower concentration of Sn^{4+} ($y = 0.1$). The response and recovery times increase with the increase in Ni^{2+} for lower concentration of Sn^{4+} ($y = 0.1$), while at higher concentration of Sn^{4+} ($y = 0.2$), there is increase (for Ni^{2+} up to $x = 0.6$) and decrease (for further increase in Ni^{2+} up to 1.0) in response and recovery times. For ethanol and Cl_2, the sensitivity of Zn FTFs decreases with an increase in Ni^{2+} and increases with an increase in Sn^{4+}. For these gases, the optimum temperature is found to be higher for higher concentration of Sn^{4+}. The response and recovery times of Zn FTFs for ethanol and Cl_2 increase with increasing Ni^{2+} and Sn^{4+}.

Electronic supplementary material The online version of this article (doi:10.1007/s10008-016-3254-z) contains supplementary material, which is available to authorized users.

✉ S. P. Dalawai
sanjeevdalawai@gmail.com

[1] Department of Electronics, Shivaji University, Kolhapur, MS 416 004, India

[2] Department of Physics, Smt KRP Kanya Mahavidyalaya, Islampur, MS 415 409, India

[3] Department of Physics, GKG College, Kolhapur, MS 416 012, India

Keywords Zn-Ni-Sn FTFs · Screen printing · Sensitivity · Optimum temperature · Response-recovery time

Introduction

Soft ferrites are one of the most important materials used in the fabrication of electronic components. They possess good chemical and thermal stability under operating conditions. Nowadays, researchers have focused their attention on gas sensors of soft ferrites. Among the soft ferrites, Ni-Zn ferrites are particularly useful because of their high resistivity, low loss and high saturation magnetization [1]. By substituting divalent, trivalent and tetravalent impurities, the properties of the soft ferrites can be changed. Kadu et al. [2] synthesized Zn-Mn ferrite sensors and tested for LPG, CH_3, CO and C_2H_5OH. They reported that Zn-Mn ferrite sensor is sensitive to ethanol at an operating temperature of 300 °C. They found improved sensitivity, response and reduced operating temperature to 230 °C with the addition of palladium in Zn-Mn ferrite sensors. Vasambekar et al. [3] studied the gas sensing properties of Nd^{3+}-substituted zinc ferrites for ethanol, Cl_2 and LPG. They reported that response and recovery decrease with an increase in Nd^{3+} content in zinc ferrite. Rezlescu et al. [4] reported the influence of partial replacement of Mg and Fe ions by Sn^{4+} and Mo^{6+} ions and studied their structural, electrical and gas sensing properties. These ferrites were more sensitive to acetone than ethanol. Doroftei et al. [5] studied the influence of Sn^{4+} and/or Mo^{6+} ions on the structure and the humidity sensitivity of Mg ferrite prepared by self-combustion method. The role of Sn^{4+} substitution in Mg ferrite is to enhance the humidity sensitivity. The improvement of resistivity, density and permeability with the addition of Sb in Ni-Zn ferrite is reported by Praveena and Srinath [6].

The study of gas sensing properties of ferrites showed very good surface reactivity. The ferrites have temperature-dependent surface morphologies [7–10]. Reddy et al. [7] prepared nanocrystalline nickel ferrite by micro-emulsion and hydrothermal methods and studied its gas sensing properties for LPG. They found that nickel ferrite prepared by the hydrothermal method shows high sensitivity at lower operating temperatures compared to that prepared by mitcelle technique. They also observed the significant reduction in operating temperature and faster response for palladium-substituted nickel ferrite. Gopal Reddy et al. [8] reported the gas sensing properties at lower concentrations of chlorine gas for nickel ferrite. Gadkari et al. [9] studied the gas sensing properties of Sm^{3+}-added Mg-Cd ferrites. They reported lower response and recovery times for Sm^{3+}-added Mg-Cd ferrites than that for Mg-Cd ferrites. They also observed that response-recovery times of Mg-Cd ferrites decrease with an increase in Cd^{2+} content.

Kamble and Mathe [10] showed that the nickel ferrite thick film (FTF) is an efficient gas sensor for chlorine compared to LPG and NH_3 at room temperature. Gawas et al. [11] prepared $Mn_{0.3}Ni_{0.3}Zn_{0.4}Fe_2O_4$ powder by autocatalytic thermal decomposition technique. They deposited thick films by the screen printing method. The sensors showed high sensitivity to NH_3 gas at room temperature and also high selectivity at 10 ppm against other toxic gases at higher concentrations. Bangale and Bamane [12] prepared Mg ferrite powders by solution combustion method and thick films by the screen printing method. They showed that these ferrites have high sensitivity and good selectivity to ethanol gas at 30 ppm compared to acetone, H_2S, CO_2 and LPG. By the similar method, zinc FTF was prepared. This nanocrystalline zinc FTF has high sensitivity and good selectivity to Cl_2 at 300 ppm compared to acetone, NH_3, H_2, H_2S and LPG [13]. They also found that zinc FTF has high sensitivity and good selectivity to H_2S gas at 1000 ppm [14].

NiO/TiO_2-added zinc ferrite gas sensor was tested by Arshak and Gaidan [15] for alcohols like ethanol, pentanol, propanol, butanol and hexanol. The sensor showed highest sensitivity to hexanol. It is observed that the addition of NiO/TiO_2 improved the response and recovery times. They also found that the response and recovery times are temperature dependent and decrease with an increase in operating temperature. Rezlescu et al. [16] prepared zinc ferrite by self-combustion method and tested its sensing properties for LPG, C_2H_5OH and CH_3COOH. They found that zinc ferrite is sensitive and selective to ethanol. Xiangfeng and Chenmou [17] prepared MFe_2O_4 (M = Zn, Cd, Mg and Cu) thick films by co-precipitation method and tested their sensing properties for H_2S, CH_3SH and $(CH_3)_2S$. They reported that $CdFe_2O_4$ is sensitive, even at 0.01 ppm concentration of CH_3SH.

Current status and future trends on solid-state potentiometric gas sensors have been reported by Pasierb and Rekas [18]. They reported that the potentiometric gas sensors may be used in a variety of areas including domestic applications, agriculture, industries, medicine, automobiles, mines, control of gas emissions, leak and fire. Mobius and Hartung [19] carried further research on potentiometric gas sensors by adding some oxygen sensors in reducing gases. Bahteeva et al. [20], Shalaeva et al. [21], Markov et al. [22] and Kharton et al. [23] synthesized strontium-substituted ferrites. They revealed that the variation in accepter doping level and oxygen vacancy concentration results in structural modifications that develop simultaneously with changes in ionic conductivity.

We reported the gas sensing properties of Y^{3+}-added nanocrystallite Mg-Cd ferrite [24] and Ni-Zn ferrite thick films [25] for LPG, ethanol and chlorine. It is clear that thick films show good sensitivity as compared to the bulk material. No literature is found for the gas sensing properties of Sn^{4+}-substituted Ni-Zn ferrites and Sn^{4+}-substituted Ni-Zn FTFs. Therefore, it was decided to prepare Ni-Zn-Sn FTFs and study their gas sensing properties for LPG, ethanol and chlorine at various operating temperatures.

Experimental

Preparation of Ni-Zn-Sn ferrite powder

The nanosize ferrite powders of $Ni_xZn_{1-x+y}Fe_{2-2y}Sn_yO_4$ (x = 0, 0.2, 0.4, 0.6, 0.8, 1.0 and y = 0.1, 0.2) system were prepared by oxalate co-precipitation method. The AR-grade $ZnSO_4.6H_2O$ (Thomas Baker), $NiSO_4.6H_2O$ (Molychem), $FeSO_4.7H_2O$ (Thomas Baker) and $SnSO_4$ (Thomas Baker) were dissolved in double-glass-distilled water in the required proportion. The pH of the solution was maintained at 4.0 by adding conc. H_2SO_4. The mixture was heated at 80 °C for 1 h to optimize the complete ionization of metal sulphates. AR-grade ammonium oxalate solution (Sd Fine-Chem. Ltd) was added with stirring until complete precipitation was obtained. The precipitate was filtered and washed several times with double-glass-distilled water in order to remove sulphate ions. The removal of sulphate ions was confirmed by barium chloride test [9, 24]. The precipitate was dried on a hot plate and pre-sintered at 200 °C for 1 h. The pre-sintered powders were milled in an agate mortar with acetone as a base and finally sintered at 450 °C for 2 h.

Ni-Zn-Sn ferrite thick film preparation

The FTFs of $Ni_xZn_{1-x+y}Fe_{2-2y}Sn_yO_4$ (x = 0, 0.2, 0.4, 0.6, 0.8, 1.0; y = 0.1, 0.2) powders having an area of 10 × 10 mm^2 were prepared by screen printing technique. Ni-Zn-Sn ferrite powders of different compositions were deposited on a glass substrate. For deposition, the mixture of 90 wt% of Ni-Zn-Sn ferrite powders with an organic binder of 5 wt% ethyl

cellulose and 5 wt% 2-(2-butoxyethoxy) ethyl acetate was used. The electrical contacts on both the ends of the thick films were made by using a silver conductive adhesive paste (AlfaAesar). The photograph of Ni-Zn-Sn FTFs (x = 0, 0.2, 0.4, 0.6, 0.8, 1.0; y = 0.1) were shown in Fig. 1.

The measurements of FTF thicknesses were carried on surface profiler Ambios Tech. XP-1 and were found in the range of 15–20 μm.

Characterization

The XRD patterns of Ni-Zn-Sn ferrite powder were recorded on (Bruker D2 phaser, USA) desktop X-ray powder diffractometer in the range of 10°–90° (2θ), a step size of 0.02° at 30 kV, 10 mA with Cu$K\alpha$ radiation (λ = 1.54184 Å). The FT-IR spectra of ferrite powders were recorded in the range of 300–800 cm^{-1} using a Perkin Elmer spectrum one spectrometer, USA, by KBr pellet technique. The surface morphology of the FTF was studied with the help of FE-SEM on Hitachi, Model: S-4700, Japan.

Gas sensing

The gas sensing behaviour of $Ni_xZn_{1-x+y}Fe_{2-2y}Sn_yO_4$ (x = 0, 0.2, 0.4, 0.6, 0.8, 1.0 and y = 0.1, 0.2) FTFs was measured by using a lab-made gas sensor unit for the gases like chlorine, ethanol and LPG by using a two-probe method. Ohmic contacts of silver paste were made for the 10 × 10 mm^2 thick films on glass substrates. A 500-ppm test gas was inserted in the chamber with the help of a syringe. The resistance of the ferrite thick film sensor in air (R_a) and in the presence of various test gases (R_g) of LPG, C_2H_5OH and Cl_2 was calculated by measuring the current flowing through the film at various temperatures.

The sensitivity of all FTF sensor elements was calculated by using relations [9, 24–25].

$$S(\%) = \frac{\Delta R}{R_a} \times 100 = \frac{|R_a - R_g|}{R_a} \times 100 \quad (1)$$

Results and discussion

Structural properties

The typical X-ray diffraction patterns of Ni-Zn-Sn (x = 0.8, 1.0; y = 0.1, 0.2) are presented in Fig. 2. The presence of (111), (220), (311), (222), (400), (422), (511), (440) and (533) planes in the figure confirms the formation of a single-phase cubic spinel structure. All the peaks in the diffraction patterns with JCPDS card number-52-0278 are in good agreement. From this figure, it is found that there is no extra peak present in the samples. The typical FE-SEM image of Ni-Zn-Sn (x = 0.6, y = 0.1) FTF is presented in Fig. 3. It is noticed that the average grain size of the samples under investigation lies in the range of 20–60 nm, highly porous nature and located in loosely packed agglomerates. The particle size of the samples decreases with an increase in Sn^{4+} content. The typical FT-IR spectrum of Ni-Zn-Sn (x = 0.8, 1.0; y = 0.1, 0.2) ferrite is presented in Fig. 4. The figure shows two major absorption bands near the high-frequency absorption band (υ_1) in the range of 596 to 568 cm^{-1} and low-frequency absorption bands (υ_2) in the range of 481 to 469 cm^{-1}. These are corresponding to intrinsic lattice vibrations of octahedral and tetrahedral sites, respectively [26].

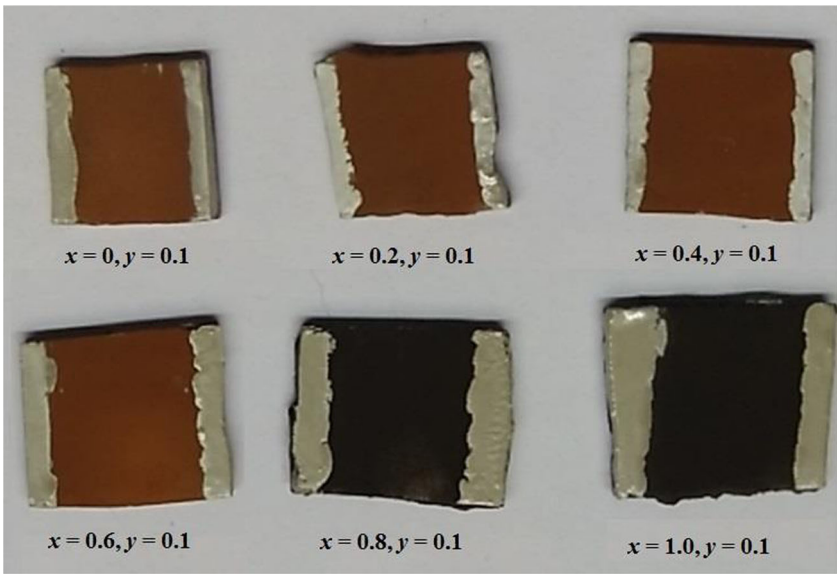

Fig. 1 Photograph of Ni-Zn-Sn FTFs (x = 0, 0.2, 0.4, 0.6, 0.8,1.0; y = 0.1)

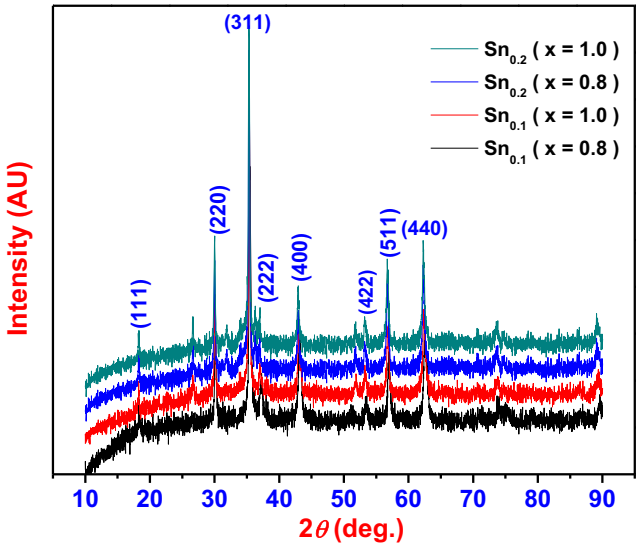

Fig. 2 Typical X-ray diffraction patterns of Ni-Zn-Sn (x = 0.8, 1.0; y = 0.1, 0.2) ferrite

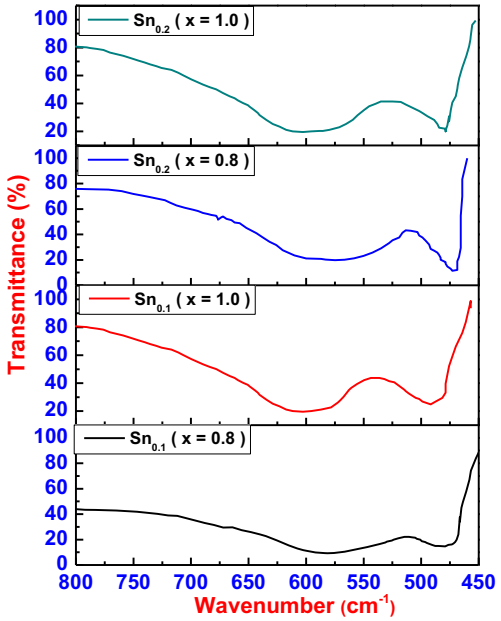

Fig. 4 Typical FT-IR spectrum of Ni-Zn-Sn (x = 0.8, 1.0; y = 0.1, 0.2) ferrite

Gas sensing properties

The gas sensing properties of the Ni-Zn-Sn FTFs were measured by laboratory-made gas sensor unit for LPG, ethanol and chlorine at a concentration of 500 ppm. The variation of sensitivity with operating temperature of Ni-Zn-Sn FTFs for LPG, ethanol and chlorine is presented in Figs. 5, 11 and 15. From these figures, it is found that the sensitivity of each FTF initially increases, reaches to a maximum, and then decreases with an increase in temperature for each test gas. This type of behaviour of sensitivity is attributed to the rate of chemical reaction and diffusion of gas molecules. For maximum sensitivity, the rate of chemical reaction and diffusion of gas molecules becomes equal. The temperature at highest sensitivity is referred to as an optimum operating temperature [24]. Such type of behaviour of the sensitivity of FTFs is reported by several researchers [10, 12–17]. The gas sensing mechanism of FTFs under investigation is depicted by the flow diagram presented in Fig. 6.

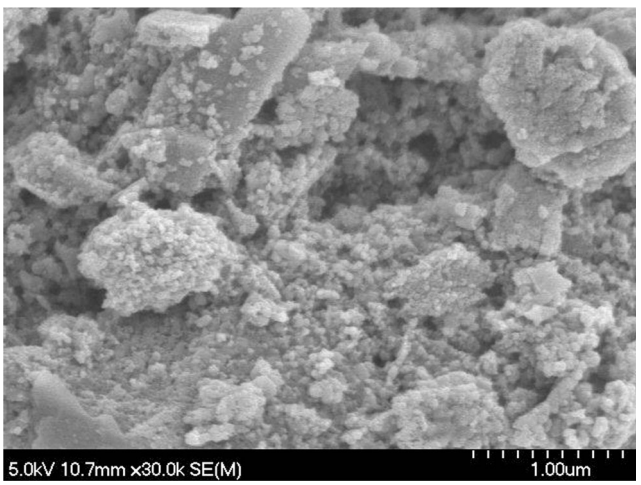

Fig. 3 Typical FE-SEM images of Ni-Zn-Sn (x = 0.6, y = 0.1) FTF

In sensors, chemisorbed oxygen species like O^-, O_2^- and O^{2-} appear on the surface and plays an important role in the gas sensing mechanism [24]. Usually, sensing mechanism depends on the operating temperature. Sensing mechanism of oxygen adsorbed on the surface of FTFs is given as [24, 34]

$$O_{2gas} \leftrightarrows O^-_{2ads} \leftrightarrows 2O^-_{ads} \leftrightarrows O^{2-}_{ads} \quad (2)$$

The reaction mechanism for reducing gases on the surface of FTFs with oxygen species is given as [17]

$$R_{(gas)} \leftrightarrows R_{(ads)} \quad (3)$$

$$R_{(ads)} + O^-_{(ads)} \leftrightarrows RO_{(ads)} + e^- \quad (4)$$

When a reducing gas reacts with chemisorbed oxygen, an electron is released back to the conduction band, resulting in changes in the resistance of a sensor.

The variation of grain size and sensitivity with nickel content for Ni-Zn-Sn FTFs is presented in Fig. 7. From this figure, it is noticed that the inverse relation between grain size and sensitivity of Ni-Zn-Sn FTFs expects the sample (x = 0.8, 0.1) for LPG. For higher concentration of Sn^{4+} (y = 0.2) content, the sensitivity of Ni-Zn-Sn FTFs becomes higher and grain size becomes lower as compared to lower concentration of Sn^{4+} content (y = 0.1).

Ni-Zn-Sn FTFs as LPG sensors

When Ni-Zn-Sn FTFs are exposed to LPG, they react with chemisorbed oxygen species and results in the formation of gaseous species and water vapours by removal of

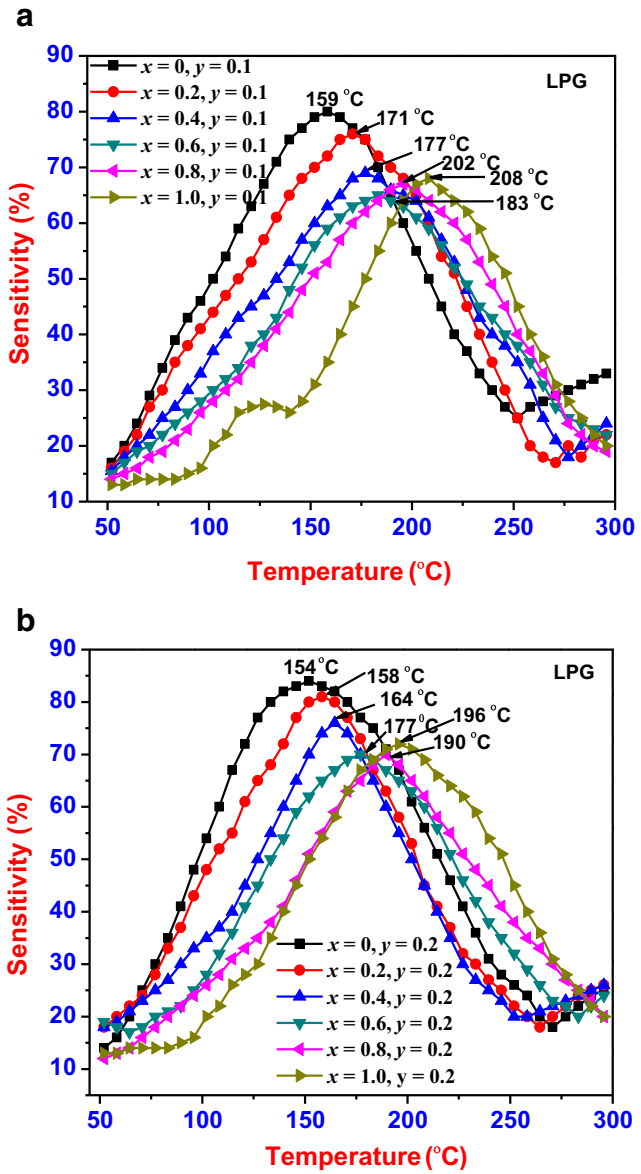

Fig. 5 Variation of sensitivity with operating temperature of **a** $Ni_xZn_{1-x+y}Fe_{2-2y}Sn_yO_4$ ($x = 0, 0.2, 0.4, 0.6, 0.8, 1.0$; $y = 0.1$) and **b** $Ni_xZn_{1-x+y}Fe_{2-2y}Sn_yO_4$ ($x = 0, 0.2, 0.4, 0.6, 0.8, 1.0$; $y = 0.2$) for LPG

adsorbed oxygen due to the interaction of hydrocarbons (C_nH_{2n+2}) of LPG.

The reaction of LPG with chemisorbed oxygen is given as

$$2C_nH_{2n+2} + 2O_2^- \leftrightarrows 2C_nH_{2n}O + 2H_2O + 2e^- \quad (5)$$

This reaction shows the increased concentration of electrons in the conduction band, resulting in the increased conductance of Ni-Zn-Sn FTFs. This was reflected in increased current after exposure to the gas as expected [24, 27].

From the plot of temperature versus sensitivity presented in Fig. 5a, b, it is observed that the sensitivity and operating temperature of Ni-Zn-Sn FTFs for LPG varies in the range of 65–84 and 154–208 °C, respectively. The variation of sensitivity and optimum temperature of Ni-Zn-Sn FTFs with nickel for LPG is presented in Fig. 8. It is seen that the sensitivity of Ni-Zn-Sn FTFs decreases with increased nickel content (up to $x = 0.6$) and slightly increases thereafter for further increment in nickel content (for $x = 0.8$ and 1.0). This change in the sensitivity may be due to the DC electrical resistivity, and activation energy of Ni-Zn-Sn FTFs decreases with increased nickel content (up to $x = 0.6$) and slightly increases thereafter for further increment in nickel content (for $x = 0.8$ and 1.0); these results are presented in Fig. S1 (in Supplementary Information). This is also due to the Yafet-Kittel model for ($x = 0.8$ and 1.0) the sensitivity increases with an increase in nickel content [27, 28]. From this plot, it can be further noticed that the sensitivity of Ni-Zn-Sn FTFs for higher concentration of Sn^{4+} ($y = 0.2$) is higher than that for lower concentration of Sn^{4+} ($y = 0.1$). This is attributed to the decreased grain size in these FTFs with increased Sn^{4+} substitution.

From this figure, it is also noticed that the optimum temperature increases with an increase in nickel content. This is due to the increasing grain size of FTFs with Ni^{2+} content. For Ni-Zn-$Sn_{0.2}$ FTFs, optimum temperature is lower than that for Ni-Zn-$Sn_{0.1}$ FTFs. It is found that there is an inverse relation between operating temperature and sensitivity in Ni-Zn-Sn FTFs till the Neel's two-sublattice model is observed (up to $x = 06$). Thereafter, for the Yafet-Kittel model ($x = 0.8$ and 1.0), the sensitivity is seen to follow the same trend of increment as that of operating temperature with increased nickel content [28, 29].

The response and recovery characteristics of Ni-Zn-Sn FTFs ($x = 0$, 0.2, 0.4, 0.6, 0.8 and 1.0; y = 0.1 and 0.2) for LPG are presented in Fig. S2 (a-b) (in Supplementary Information). From Fig. S2, it is found that the response and recovery time lies in the range of 10–28 and 20–37 s, respectively, for lower ($y = 0.1$) and higher ($y = 0.2$) concentrations of Sn^{4+}.

The variation of response and recovery times of Ni-Zn-Sn FTFs ($x = 0$, 0.2, 0.4, 0.6, 0.8,1.0; y = 0.1 and 0.2) with nickel content for LPG is presented in Fig. 9. From this figure, it is noticed that the response and recovery times for lower concentration of Sn^{4+} ($y = 0.1$) increase with increasing nickel content. However, for higher concentration of Sn^{4+} ($y = 0.2$), the response and recovery times increase with an increase in nickel content (up to $x = 0.6$, i.e. till the Neel's two-sublattice is dominant) [28, 29]. Thereafter, there is a decrement in the response and recovery times for further increase in nickel content ($x = 0.8$ and 1.0, i.e. for the predominance of Yafet-Kittel model) [28, 29] for higher concentration of Sn^{4+}. It is also observed that the response and recovery times of Ni-Zn-Sn FTFs for higher concentration of Sn^{4+} ($y = 0.2$) are lower than that for lower concentration of Sn^{4+} ($y = 0.1$).

The Ni-Sn FTF sensor shows short response (10 s) and good recovery time (20 s) for LPG.

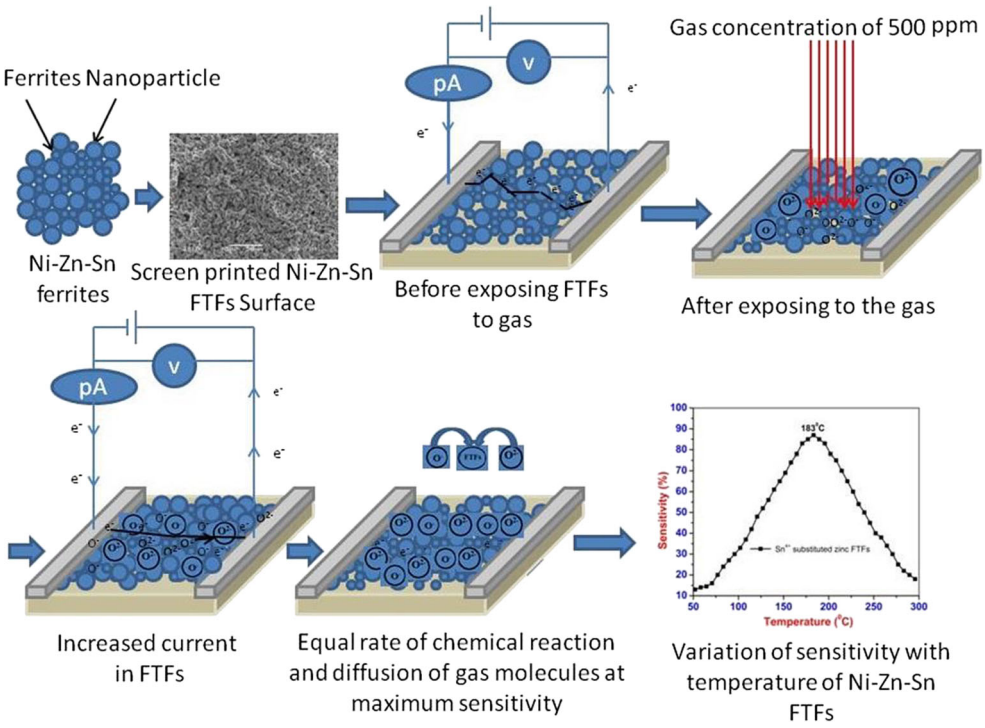

Fig. 6 The layout of the gas sensor mechanism of FTFs

Ni-Zn-Sn FTFs as an ethanol sensor

When Ni-Zn-Sn FTFs are exposed to ethanol, the reaction with chemisorbed oxygen species on the surface is given as [30, 31]

$$C_2H_5OH_{gas} + O^{2-}_{ads} \rightarrow C_2H_5O^{-}_{(ads)} + OH^{-}_{ads} \quad (6)$$

$$C_2H_5O^{-}_{(ads)} \rightarrow (C_2H_5)O_{ads} + O^{-}_{ads} + e^{-} \quad (7)$$

$$C_2H_5OH_{gas} + O^{2-}_{ads} + \text{hole} \rightarrow CO_2 + H_2O + V_o^{\bullet\bullet} \quad (8)$$

In these reactions, ethanol is adsorbed by the oxygen species ($O_{(ads)}^{2-}$) and produces adsorbed gas species ($C_2H_5O_{(ads)}^{-}$), along with a hydroxide group. Adsorbed gas species further gives gaseous species and an electron. The ethanol gas is exposed to chemisorbed oxygen species and hole to produce carbon dioxide, water molecules and doubly charged oxygen vacancy ($V_o^{\bullet\bullet}$). During the sensing mechanism of gas with the surface of FTFs, electrons enters in the conduction band, leading to decrease the resistance of Ni-Zn-Sn FTFs [30, 31].

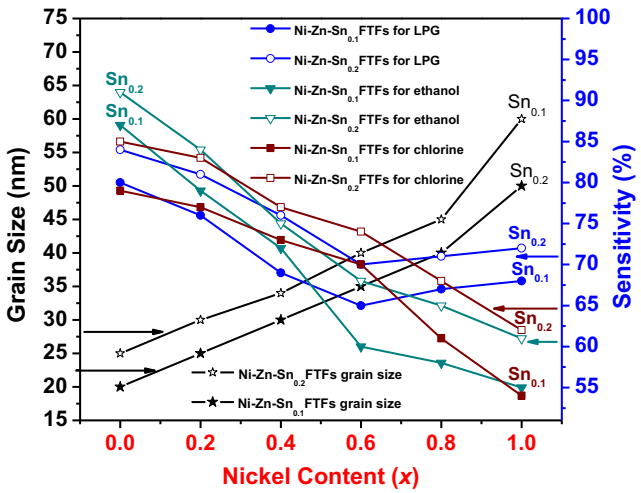

Fig. 7 Variation of grain size and sensitivity with nickel content for $Ni_xZn_{1+y-x}Fe_{2-2y}Sn_yO_4$ ($x = 0, 0.2, 0.4, 0.6, 0.8, 1.0$; $y = 0.1, 0.2$)

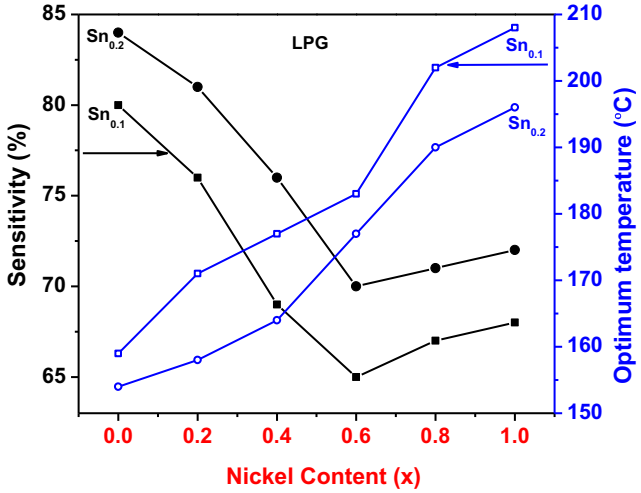

Fig. 8 Variation of sensitivity and optimum temperature of Ni-Zn-Sn FTFs with nickel content for LPG

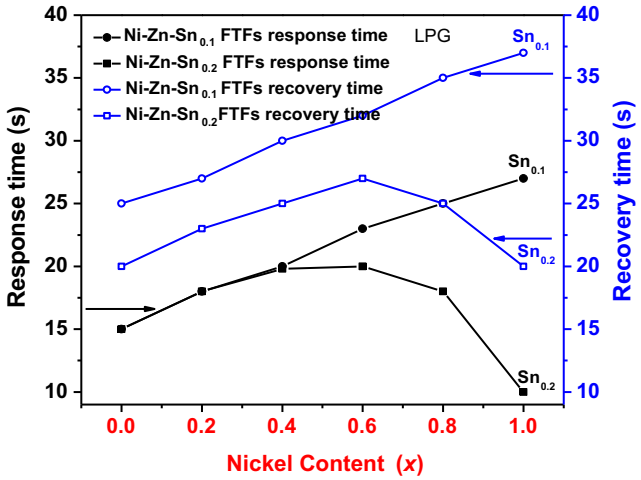

Fig. 9 Variation of response and recovery times of Ni-Zn-Sn FTFs with nickel content for LPG

The variation of sensitivity with operating temperature of Ni-Zn-Sn FTFs (x = 0, 0.2, 0.4, 0.6, 0.8, 1.0; y = 0.1, 0.2) for ethanol is presented in Fig. 10a, b. From these figures, it is revealed that the sensitivity and optimum temperature of Ni-Zn-Sn FTFs lies in the range of 55–91 and 152–183 °C, respectively. The variation of sensitivity and optimum temperature of Ni-Zn-Sn FTFs (x = 0, 0.2, 0.4, 0.6, 0.8, 1.0; y = 0.1, 0.2) with a nickel content for ethanol is presented in Fig. 11. From this figure, it is noticed that the sensitivity and the optimum temperature of Ni-Zn-Sn FTFs decrease with an increase in nickel content. This is due to the increase in grain size of the FTFs with an increase in Ni^{2+} content (Fig. 7). It is observed that the Zn-Sn FTF has high sensitivity (91 %) to ethanol. It means that the Zn-Sn FTFs strongly interact with ethanol as compared to other FTFs [32]. The Ni-Zn FTFs with higher concentration of Sn^{4+} (y = 0.2) show lower operating temperature and higher sensitivity to ethanol compared to that with a lower concentration of Sn^{4+} (y = 0.1). The decrement of operating temperature is due to the decrease in grain size of FTFs (Fig. 7) [24, 33]. Kapse et al. [30] reported that the higher sensitivity and lower operating temperature for Pd (1.0 wt%) doped $Ni_{0.6}Zn_{0.4}Fe_2O_2$ as compared to $Ni_{0.6}Zn_{0.4}Fe_2O_2$ for ethanol.

The variation of response and recovery characteristics of Ni-Zn-Sn FTFs for ethanol is presented in Fig. S3 (a-b) (in supplementary Information). From these figures, it is found that the response and recovery times lie in the range of 10–25 and 20–40 s, respectively. The variation of response and recovery times of Ni-Zn-Sn FTFs with a nickel content of ethanol is presented in Fig. 12. The response and recovery times of Ni-Zn-Sn FTFs increase with increasing nickel content and decreases with increasing Sn^{4+} content. This is due to the increment and decrement of grain size with substitution of Ni^{2+} and Sn^{4+} in FTFs (Fig. 7).

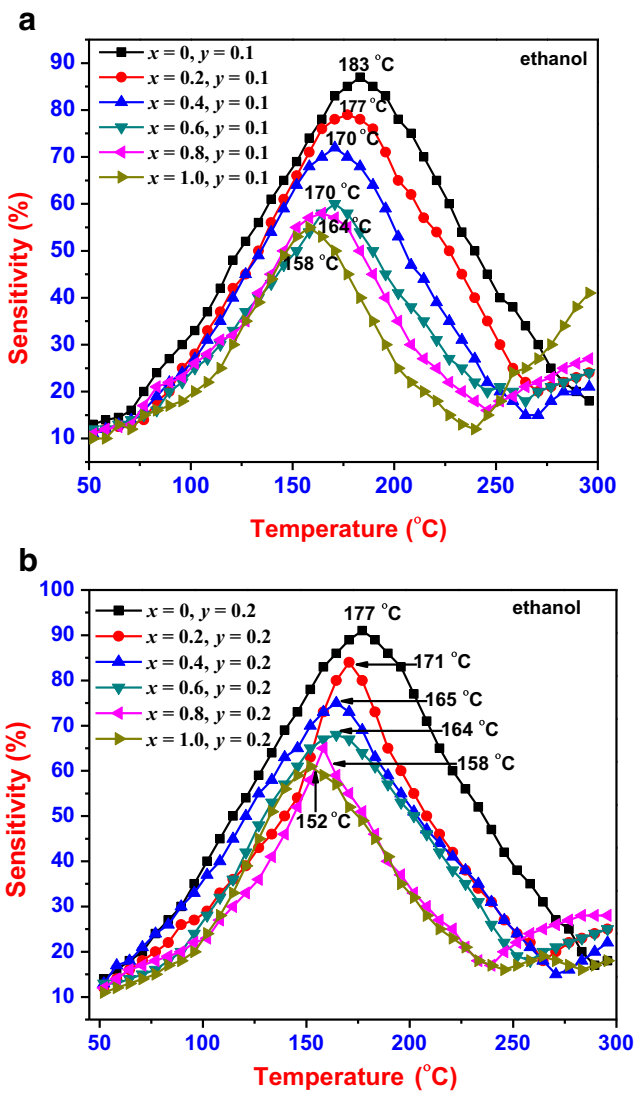

Fig. 10 Variation of sensitivity with operating temperature of **a** $Ni_xZn_{1+y-x}Fe_{2-2y}Sn_yO_4$ (x = 0, 0.2, 0.4, 0.6, 0.8, 1.0; y = 0.1) and **b** $Ni_xZn_{1+y-x}Fe_{2-2y}Sn_yO_4$ (x = 0, 0.2, 0.4, 0.6, 0.8, 1.0; y = 0.2) for ethanol

Ni-Zn-Sn FTFs as a chlorine sensor

Exposure of Ni-Zn-Sn FTFs to chlorine results in the formation of chlorides. The reaction of chlorine with the surface of FTFs is given as [10, 34]

$$Cl_2 + 2O^{2-}_{surf} \leftrightarrows 2Cl^{-}_{surf} + O_2 + 2e^{-} \quad (9)$$

$$Cl_2 + 2O^{x}_{o} \leftrightarrows 2Cl^{\prime}_{o} + O_2 + 2e^{\prime} \quad (10)$$

The reactions (9) and (10) represent an electron donation to the conduction band of Ni-Zn-Sn FTF sensor indicating decreased resistance [10].

The variation of sensitivity with operating temperature of Ni-Zn-Sn FTFs for chlorine is as presented in Fig. 13a, b. The sensitivity and operating temperature of Ni-Zn-Sn FTFs lies in the range of 54–85 and 146–202 °C, respectively.

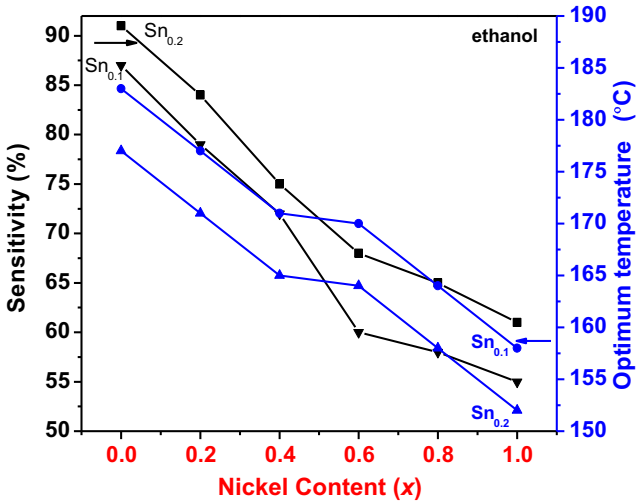

Fig. 11 Variation of sensitivity and optimum temperature of Ni-Zn-Sn FTFs with nickel content for ethanol

The variation of sensitivity and optimum temperature of Ni-Zn-Sn FTFs with a nickel content for chlorine is presented in Fig. 14. From this figure, it is revealed that the sensitivity of FTFs decreases, whereas optimum temperature increases with increasing nickel content. The increase in optimal temperature and decrease in sensitivity are mainly affected due to smaller surface area and greater grain size of FTFs under investigation (Fig. 7).

From Fig. 14, it is also observed that the sensitivity of each FTFs is higher whereas the optimum temperature of each FTFs becomes lower for higher concentration of Sn^{4+} ($y = 0.2$) in Ni-Zn FTFs than that for lower concentration of Sn^{4+} ($y = 0.1$). It is found that the optimum temperature for Ni-Zn-Sn FTFs ($x = 0$, 0.2; $y = 0.1$, 0.2) is the same, but the sensitivity is slightly different. This can be attributed to the lattice constant of Sn^{4+}-substituted Zn FTFs [35].

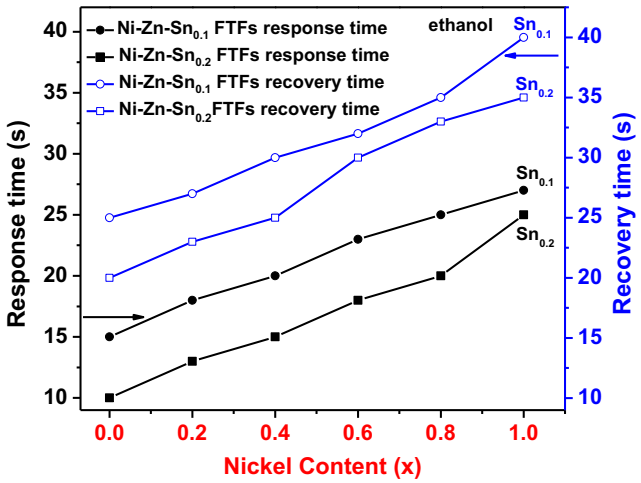

Fig. 12 Variation of response and recovery time of $Ni_xZn_{1+y-x}Fe_{2-2y}Sn_yO_4$ FTFs with nickel content for ethanol

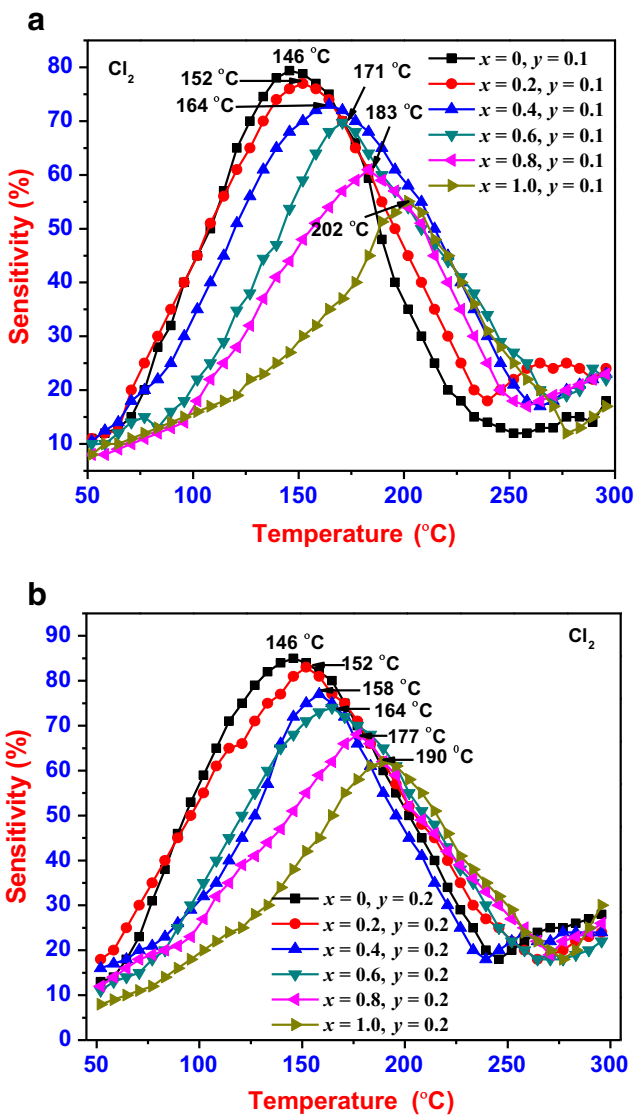

Fig. 13 Variation of sensitivity with operating temperature of **a** $Ni_xZn_{1+y-x}Fe_{2-2y}Sn_yO_4$ ($x = 0$, 0.2, 0.4, 0.6, 0.8, 1.0; $y = 0.1$) and **b** $Ni_xZn_{1+y-x}Fe_{2-2y}Sn_yO_4$ ($x = 0$, 0.2, 0.4, 0.6, 0.8, 1.0; $y = 0.2$) for chlorine

Response and recovery characteristics of Ni-Zn-Sn FTFs for chlorine are presented in Fig. S4 (a-b) (in supplementary Information). From these Fig S4, it is seen that the response and recovery times of Ni-Zn-Sn FTFs lie in the range of 10–30 and 20–35 s, respectively. The variation of response and recovery times of Ni-Zn-Sn FTFs with a nickel content for chlorine is presented in Fig. 15. From this figure, it is clear that the response and recovery times of Ni-Zn-Sn FTFs increase with increasing nickel content. The response and recovery times of Ni-Zn-Sn FTFs for higher concentration of Sn^{4+} ($y = 0.2$) are lower than that for lower concentration of Sn^{4+} ($y = 0.1$). This is due to decrement in the grain size for increased concentration of Sn^{4+}. The Sn^{4+}-substituted Zn FTF sensor under investigation has a short response (10 s) and good recovery time (15 s) for chlorine compared to other FTFs.

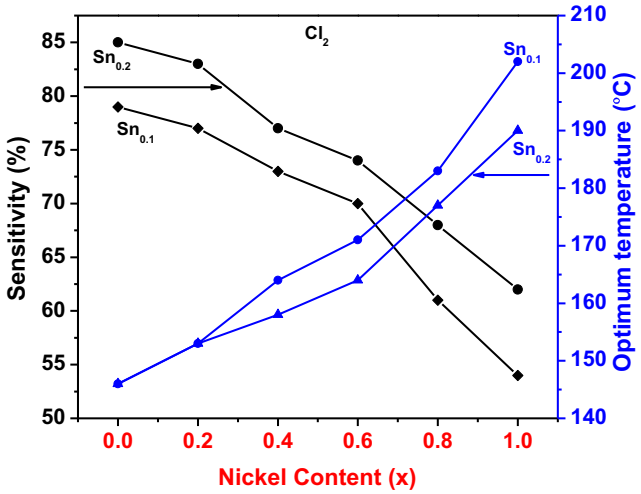

Fig. 14 Variations of sensitivity and optimum temperature of $Ni_xZn_{1+y-x}Fe_{2-2y}Sn_yO_4$ ($x = 0, 0.2, 0.4, 0.6, 0.8, 1.0$; $y = 0.1, 0.2$) with nickel content for chlorine

From Figs. 8, 11 and 14, it is clear that the sensitivity of all the ferrites decreases with an increase in Ni^{2+} content for test gases like LPG, ethanol and Cl_2. This is attributed to the increase in grain size of the Ni-Zn-Sn ferrites with the increase in Ni^{2+} content. From these figures, it is also observed that optimum temperature of the FTFs increases with the increase in Ni^{2+} content for LPG and chlorine except ethanol.

The compositional variation of sensitivity of Ni-Sn, $Ni_{0.6}Zn_{0.4}Sn$ and Zn-Sn FTFs for test gases is presented in Fig. 16. From this figure, it is confirmed that the sensitivity of Zn-Sn FTF is higher for ethanol gas as compared to the other gases like LPG and ethanol. Response and recovery time of these FTFs is also well as compared to other FTFs (Fig. 12). Therefore, Zn-Sn FTFs is highly sensitive as compared to Ni-Sn and $Ni_{0.6}Zn_{0.4}Sn$ FTFs.

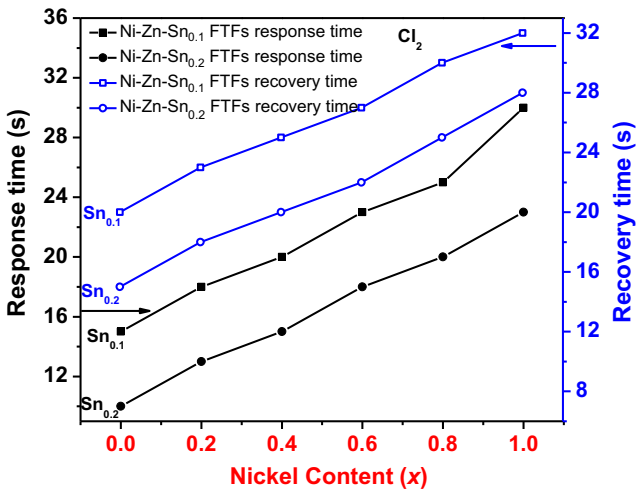

Fig. 15 Variations of response and recovery time with nickel content of Ni-Zn-Sn FTFs ($x = 0, 0.2, 0.4, 0.6, 0.8, 1.0$; $y = 0.1, 0.2$) for chlorine

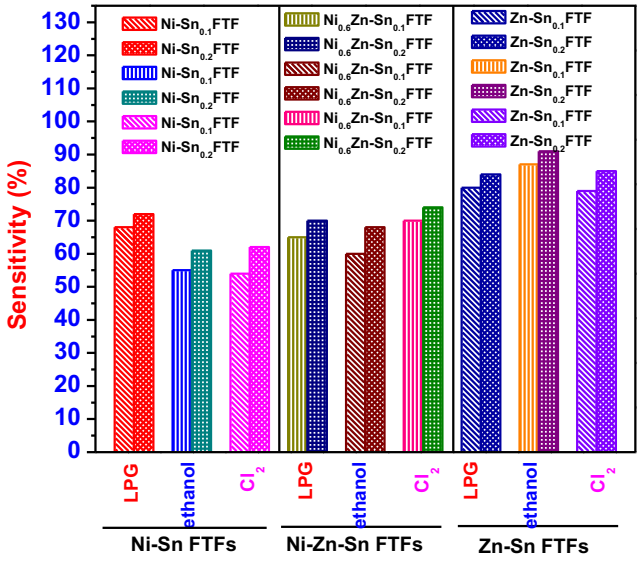

Fig. 16 Variation of sensitivity of Ni-Zn-Sn FTFs ($x = 0, 0.6, 1.0$; $y = 0.1, 0.2$) for LPG, ethanol and chlorine

Conclusions

Nanosize Ni-Zn-Sn ferrite powders were prepared by oxalate co-precipitation method. The FTFs were deposited on a glass substrate by a screen printing technique. The XRD study confirms the formation of cubic spinel structure. The FT-IR spectra confirm the formation of ferrites. From the gas sensing characteristics of the FTFs under investigation, it can be concluded that

1. The sensitivity of Ni-Zn-Sn FTFs is in the order of ethanol > Cl_2 > LPG.
2. The highest response (91 %) is shown by Zn-Sn FTFs to ethanol.
3. The lowest response (61 %) is shown by Ni-Sn FTFs to ethanol.
4. The sensitivity of Ni-Zn-Sn FTFs decreases with increases in Ni^{2+} content for ethanol and chlorine. It is attributed to increases in grain size to increase in Ni^{2+} content.
5. The sensitivity of Ni-Zn-Sn FTFs for all test gases is higher for higher concentration of Sn^{4+} ($y = 0.2$) in Ni-Zn FTFs than that for lower concentration of Sn^{4+} ($y = 0.1$). The high sensitivity is due to its smaller grain size in Sn^{4+} ($y = 0.2$) compared to that of Sn^{4+} ($y = 0.1$) Ni-Zn FTFs.
6. The response and recovery times of Ni-Zn-Sn FTFs increase with increasing Ni^{2+} content, and response and recovery time decreases with increasing Sn^{4+} concentrations.
7. The optimum temperature of Ni-Sn-Zn FTFs increases with increases in nickel content for LPG and chlorine. The optimum temperature of Ni-Zn-Sn FTFs for all test gases was decreased with the increase in Sn^{4+} concentrations.

Acknowledgments S.P. Dalawai thanks the Department of Electronics, Shivaji University, Kolhapur, for giving financial assistance through the 'Golden Jubilee Research Fellowship' in 2012–2015.

References

1. Deka S, Joy PA (2007) Enhanced permeability and dielectric constant of Ni-Zn ferrite synthesized in nanocrystalline form a combustion method. J Am Ceram Soc 90:1494–1499
2. Kadu AV, Jagtap SV, Chaudhari QN (2009) Studies on the preparation and ethanol gas sensing properties of spinel $Zn_{0.6}Mn_{0.4}Fe_2O_4$ nanomaterials. Curr Appl Phys 9:1246–1251
3. Vasambekar PN, Gadkari AB, Shinde TJ (2013) Nd^{3+} substituted nanocrystalline zinc ferrite sensors for ethanol, LPG and chlorine. Appl Mech Mater 310:150–153
4. Rezlescu N, Dorofti C, Rezlescu E, Popa PD (2006) The influence of Sn^{4+} and/or Mo^{6+} ions on the structure, electrical and gas sensing properties of Mg-ferrite. Phys Status Solidi 203:306–316
5. Doroftei C, Reszlescu E, Rezlescu N, Popa PD (2006) Microsturcture and humidity sensitive properties of $MgFe_2O_4$ ferrite with Sn and Mo substitutions prepared by self combustion method. J Optoelectron Adv Mater 8:1012–1015
6. Praveena K, Srinath S (2013) The effect of Sb on the electrical and magnetic properties of Ni-Zn ferrite prepared by so-gel auto combustion method. J Electroceram 31:168–175
7. Reddy KM, Satyanarayana L, Manorama SV, Misra RDK (2004) A comparative study of the gas sensing behavior of nanostructured nickel ferrite synthesized by hydrothermal and reverse micelle technique. Mater Res Bull 39:1491–1498
8. Gopal Reddy CV, Manorma SV, Rao VJ (1999) Semiconducting gas sensor for chlorine based on inverse spinel nickel ferrite. Sensors Actuators B Chem 55:90–95
9. Gadkari AB, Shinde TJ, Vasambekar PN (2013) Effect of Sm^{3+} ion addition on gas sensing properties of $Mg_{1-x}Cd_xFe_2O_4$. Sensors Actuators B Chem 178:34–39
10. Kamble RB, Mathe VL (2008) Nanocrystalline nickel ferrite thick film as an efficient gas sensor at room temperature. Sensors Actuators B Chem 131:205–209
11. Gawas UB, Verenkar VMS, Patil DR (2011) Nanostructured ferrite based electronics nose sensitive to ammonia at room temperature. Sens Transd J 134:45–55
12. Bangale SV, Bamane SR (2012) Nanostructured $MgFe_2O_4$ thick film resistors as ethanol gas sensors operable at room temperature. Sens Transd J 137:176–188
13. Bangale SV, Patil DR, Bamane SR (2011) Nanostructured spinel $ZnFe_2O_4$ for the detection of chlorine gas. Sens Transd J 134:107–119
14. Bangale SV, Bamane SR (2012) Preparation and study of H_2S gas sensing behaviour of $ZnFe_2O_4$ thick film resistors. Sens Transd J 137:123–136
15. Arshak K, Gaidan L (2006) Effect of NiO/TiO_2 addition in $ZnFe_2O_4$ based gas sensors in the form of polymer thick films. Thin Solid Films 495:292–298
16. Rezlescu N, Rezlescu E, Tudorache F, Popa PD (2007) Some spinel oxide compounds reducing gas sensors. Sens Transd J 78:1134–1142
17. Xiangfeng C, Chenmou Z (2003) Sulfide-sensing characteristics of MFe_2O_4 (M = Zn, Cd, Mg and Cu) thick film prepared by co-precipitation method. Sensors Actuators B Chem 96:504–508
18. Pasierb P, Rekas M (2009) Solid-state potentiometric gas sensors-current status and future trends. J Solid State Electrochem 13:3–25
19. Möbius HH, Hartung R (2010) Solid-state potentiometric gas sensors—a supplement. J Solid State Electrochem 14:669–673
20. Bahteeva JA, Leonidov IA, Patrakeev MV, Mitberg EB, Kozhevnikov VL, Poeppelmeier KR (2004) High-temperature ion transport in $La_{1-x}Sr_xFeO_{3-\delta}$. J Solid State Electrochem 8:578–584
21. Shalaeva EV, Patrakeev MV, Markov AA, Tyutyunnik AP, Murzakaev AM, Kharton VV, Tsipis EV, Waerenborgh JC, Leonidov IA, Kozhevnikov VL (2015) Ion transport in dual-phase $SrFe_{1-x}Ta_xO_{3-\delta}$ ($x = 0.03 - 0.10$): effects of redox cycling. J Solid State Electrochem 19:841–849
22. Markov AA, Chesnokov KY, Patrakeev MV, Leonidov IA, Chukin AV, Leonidova ON, Kozhevnikov VL (2016) Oxygen non-stoichiometry and mixed conductivity of $La_{0.5}Sr_{0.5}Fe_{1-x}Mn_xO_{3-\delta}$. J Solid State Electrochem 20:225–234
23. Kharton VV, Kovalevsky AV, Tsipis EV, Viskup AP, Naumovich EN, Jurado JR, Frade JR (2002) Mixed conductivity and stability of A-site-deficient Sr (Fe,Ti)O_3–dperovskites. J Solid State Electrochem 7:30–36
24. Gadkari AB, Shinde TJ, Vasambekar PN (2012) Y^{3+} added nanocrystallite Mg-Cd ferrite LPG, Cl_2 and C_2H_5OH sensors. Sens Transd J 146:110–120
25. Dalawai SP, Shinde TJ, Gadkari AB, Vasambekar PN (2015) Ni-Zn ferrite thick film gas sensors. J Mater Sci Mater Electron 26:9016–9025
26. Waldron RD (1955) Infrared spectra of ferrites. Phys Rev 99:1727–1735
27. Gedam NN, Kadu AV, Padole PR, Bodade AB, Chaudhari GN (2009) Structural properties of nanosized $NiFe_2O_4$ for LPG sensor. Sens Transd J 110:86–95
28. Satya Murthy NS, Natera MG, Youssef SI, Begum RJ (1969) Yafet-Kittel angles in zinc-nickel ferrites. Phys Rev 181:969–977
29. Shinde TJ, Gadkari AB, Vasambekar PN (2013) Magnetic properties and cation distribution study of nanocrystalline Ni-Zn ferrites. J Magn Magn Mater 333:152–155
30. Kapse VD, Ghosh SA, Raghuwanshi FC, Kapse SD, Khandekar US (2009) Nanocrystalline $Ni_{0.6}Zn_{0.4}Fe_2O_4$: a novel semiconducting material for ethanol detection. Talanta 78:19–25
31. Sun Z, Liu L, Jia DZ, Pan W (2007) Simple synthesis of $CuFe_2O_4$ nanoparticles as gas sensing materials. Sensors Actuators B Chem 25:144–148
32. Rezlescu N, Reszlescu E, Tudirache F, Popa PD (2009) Gas sensing properties of porous Cu-,Cd- and Zn-ferrites. Rom Rep Phys 61:223–234
33. Gadkari AB, Shinde TJ, Vasambekar PN (2011) Ferrite gas sensors. IEEE Sensors J 11:849–861
34. Dawson DH, Williams DE (1996) Gas-sensitive resistors: surface interaction of chlorine with semiconducting oxides. J Mater Chem 6:406–414
35. Lee JY, Lee GJ, Kim HS, Lee SH, Lee DH, Yo CH, Kim KH, Ahn K (1998) Electrical and magnetic properties of the Sn^{4+} substituted spinel ferrite, $ZnSn_xFe_{2-4x/3}O_4$ ($0.00 \le x \le 0.30$). Mater Chem Phys 52:267–271